

Article

Taxis of Artificial Swimmers in a Spatio-Temporally Modulated Activation Medium

Alexander Geiseler ^{1,*}, Peter Hänggi ^{1,2,3} and Fabio Marchesoni ^{4,5}

¹ Institute of Physics, University of Augsburg, D-86135 Augsburg, Germany; hanggi@physik.uni-augsburg.de

² Nanosystems Initiative Munich, Schellingstraße 4, D-80799 München, Germany

³ Department of Physics, National University of Singapore, 117551 Singapore, Singapore

⁴ Center for Phononics and Thermal Energy Science, School of Physics Science and Engineering, Tongji University, Shanghai 200092, China; fabio.marchesoni@pg.infn.it

⁵ Dipartimento di Fisica, Università di Camerino, I-62032 Camerino, Italy

* Correspondence: alexander.geiseler@physik.uni-augsburg.de; Tel.: +49-821-598-3251

Academic Editors: Giancarlo Franzese, Ivan Latella and Miguel Rubi

Received: 19 January 2017; Accepted: 27 February 2017; Published: 3 March 2017

Abstract: Contrary to microbial taxis, where a tactic response to external stimuli is controlled by complex chemical pathways acting like sensor-actuator loops, taxis of artificial microswimmers is a purely stochastic effect associated with a non-uniform activation of the particles' self-propulsion. We study the tactic response of such swimmers in a spatio-temporally modulated activating medium by means of both numerical and analytical techniques. In the opposite limits of very fast and very slow rotational particle dynamics, we obtain analytic approximations that closely reproduce the numerical description. A swimmer drifts on average either parallel or anti-parallel to the propagation direction of the activating pulses, depending on their speed and width. The drift in line with the pulses is solely determined by the finite persistence length of the active Brownian motion performed by the swimmer, whereas the drift in the opposite direction results from the combination of the ballistic and diffusive properties of the swimmer's dynamics.

Keywords: microswimmers; taxis; inhomogeneous activating medium

1. Introduction

The directed movement of microorganisms, such as bacteria or cells, induced by an external stimulus is called taxis. It is categorized based on the nature of the stimulus and on whether the microorganisms head toward (positive taxis) or away (negative taxis) from the stimulus' source [1]. Commonly, taxis is induced by certain chemicals (chemotaxis) or light (phototaxis), but alternative tactic mechanisms are also known, like rheotaxis, the response to fluid flows, or gravitaxis, the response to the gravitational field [2]. Taxis plays a major role in many biological processes, e.g., in the formation of cell layers and other biological structures. Moreover, many bacteria profit from pronounced tactic capabilities in their search for food or escape from toxic substances [3,4]. They do so by means of a built-in chemical signaling network, which elaborates their physiological response to external stimulus gradients [5].

A biomimetic counterpart of microbial motility is the self-propulsion of artificial microswimmers, synthetically fabricated microparticles that propel themselves by converting an external activating "fuel" into kinetic energy [6–9]. Under certain operating conditions, such particles generate local non-equilibrium conditions in the suspension medium, which in turn exerts on them a thermo- [10–13], electro- [14,15] or diffusiophoretic [16–18] push. Because the ability to control the transport of such particles is emerging as a key task in nanorobotic applications, rectification of artificial microswimmers is currently the focus of intense cross-disciplinary research. Unlike biological microorganisms, simple

artificial microswimmers lack any internal sensing mechanism and, thus, cannot detect an activation gradient, with their response to the activating stimulus being instantaneous. Nevertheless, over the past few years, artificial microswimmers have been reported to undergo a tactic drift when exposed to static stimuli [19–23]. In biological systems, however, tactic stimuli are seldom static, but more frequently modulated in the form of spatio-temporal signals, like traveling wave pulses. Some microorganisms are capable of locating the pulse source and heading toward it [24,25]. This is an apparently paradoxical effect, because one expects rectification to naturally occur in the opposite direction, irrespective of the microorganisms' tactic response to a monotonic gradient. Indeed, assuming a symmetric pulse waveform, a microorganism orients itself parallel to the direction of the pulse propagation on one side of the pulse, and opposite to it on the other side. As the swimmer spends a longer time within the pulse when moving parallel to it, one would then expect it to “surf” the pulse and effectively move away from the pulse's source (Stokes' drift [26,27]). Experimental evidence to the contrary has been explained by invoking a finite adaption time of the microorganisms' response to temporally varying stimuli [28,29].

By analogy with the taxis of “smart” adaptive biological swimmers, in a recent paper [30], we investigated the question of whether similar effects can be observed also for “dumb” artificial swimmers, that is we considered a self-propelled particle subjected to traveling activation wave pulses. We numerically found that the particle drifts on average either parallel or anti-parallel to the incoming wave, the actual direction depending on the speed and width of the pulses. This behavior is a consequence of the spatio-temporal modulation of the particle's self-propulsion speed within the activating pulses. We complement now that first report by deriving new analytical results for the tactic drift of an artificial swimmer. For this purpose, in Section 2, we review the results of [30]. In Section 3, we then focus on two limiting cases of the swimmer's dynamics, where an analytical treatment is viable. We conclude with a brief résumé in Section 4.

2. Artificial Microswimmers Activated by Traveling Wave Pulses

At low Reynolds numbers, the dynamics of an artificial microswimmer diffusing on a 2D substrate and subjected to a spatio-temporally modulated activation can be modeled by the Langevin equations (LEs) [30]:

$$\begin{aligned}\dot{x} &= v(x, t) \cos \phi + \sqrt{D_0} \xi_x(t), \\ \dot{y} &= v(x, t) \sin \phi + \sqrt{D_0} \xi_y(t), \\ \dot{\phi} &= \sqrt{D_\phi} \xi_\phi(t).\end{aligned}\tag{1}$$

Here, $v(x, t)$ is the particle's self-propulsion velocity and ϕ denotes its orientation measured with respect to the x axis. The above dynamics comprises three additive fluctuational noise sources—two translational of intensity D_0 and one rotational of intensity D_ϕ —which, for simplicity, are represented by white Gaussian noise processes with zero mean and autocorrelation functions $\langle \xi_i(t) \xi_j(0) \rangle = 2\delta_{ij}\delta(t)$ for $i, j = x, y, \phi$, as usually assumed in the current literature [9]. The noises $\xi_i(t)$ model the combination of independent fluctuations, namely the thermal fluctuations in the swimmer's suspension fluid and the fluctuations intrinsic to its self-propulsion mechanism. Therefore, in the following, we treat D_0 and D_ϕ as independent parameters. We remind that in the presence of the sole thermal fluctuations, for a spherical particle of radius R , the translational and rotational diffusion constants are related, that is $D_0/D_\phi = 4R^2/3$ [31].

When the swimmer's activation is not modulated, its self-propulsive velocity is nearly constant, i.e., $v(x, t) \rightarrow v_0$, and the particle performs an active Brownian motion with persistence time $\tau_\phi = D_\phi^{-1}$ and corresponding persistence length $l_\phi = v_0 \tau_\phi$. On short timescales, its dynamics is then characterized by a directed ballistic motion and on long timescales by an enhanced diffusion with zero shift and diffusion constant $\lim_{t \rightarrow \infty} \langle [x(t) - x(0)]^2 \rangle / (2t) = D_0 + D_s$, where $D_s = v_0^2 / (2D_\phi)$ [32].

In Equation (1), we assumed the swimmer's self-propulsion velocity, $v(x, t)$, to be a local function of the activating "fuel" concentration, which in turn can be modulated in time and space. An ideal setup allowing for the creation of traveling activation pulses is illustrated in Figure 1a. In this sketch, a thermophoretic swimmer activated by laser light [11,18] is placed on a 2D substrate. Traveling wave pulses of laser intensity I can be generated by sliding at constant speed u a slit screen placed between the laser source and the particle. Because in a wide range of I , the swimmer's self-propulsive velocity is approximately proportional to the laser intensity [12], one thus can generate any desired profile for $v(x, t)$. Although this is probably the simplest way to experimentally realize traveling activation pulses, we remark that chemically activated swimmers represent a viable option, as well. Indeed, such swimmers can be operated under the condition that $v(x, t)$ is proportional to the concentration of the activating chemical(s), whereas their rotational diffusivity remains almost constant [17,33]. On the other hand, traveling chemical waves can be conveniently excited in chemical reactors [34–36].

The effect of a single Gaussian activation pulse, $v(x, t) = v_0 \exp[-(x - ut)^2 / (2L^2)]$, hitting the swimmer from the left is depicted in Figure 1b. Clearly, a pulse speed $u \ll v_0$ causes the particle to shift to the left, $\Delta(t) := \langle x(t) - x(0) \rangle < 0$, whereas a pulse speed of about the same magnitude as the swimmer's maximum propulsion speed, v_0 , causes it to shift slightly to the right. Indeed, we observe the final shift in the particle's position, $\Delta(\infty) = \lim_{t \rightarrow \infty} \Delta(t)$, to attain a positive maximum at $u \simeq v_0$ and tend toward large negative values for $u \rightarrow 0$. As discussed in more detail in Section 3, $\Delta(\infty)$ actually diverges in this limit if translational noise is neglected, $D_0 = 0$.

The existence of two opposing tactic regimes can be explained by considering the modulation of the swimmer's dynamics under the wave crests. Assuming no translational fluctuations, $D_0 = 0$, the swimmer can only diffuse within the pulse and comes to rest outside of it. For slow pulses, $u \ll v_0$, it propels very quickly (compared to the pulse speed) in the wave center and, thus, quickly hits either pulse's edges, defined as the points where u equals $v(x, t)$. Due to its movement to the right, the pulse's symmetry is dynamically broken, and the two edges are not equivalent: if the swimmer crosses the right edge, it becomes slower than u and is recaptured by the traveling pulse, whereas by the same argument, it is left behind by the pulse once it crosses the left edge. The right (left) edge thus behaves like a reflecting (absorbing) boundary, which allows the particle to exit the pulse on the left only, hence inducing a negative tactic shift. For pulse speeds approaching v_0 , a contrasting effect comes into play: within the pulse, the particle can travel a longer distance to the right than to the left. This "surfing" behavior, already mentioned in Section 1, is most pronounced at $u = v_0$, where the distance a swimmer can travel to the right without hitting a pulse edge is solely limited by its rotational diffusivity, D_ϕ . Accordingly, $\Delta(\infty)$ turns positive if u becomes comparable to v_0 and vanishes monotonically in the limit $u \rightarrow \infty$, where the pulse sweeps through the swimmer so quickly that it cannot respond. We note that the latter argument holds also for $D_0 \neq 0$; as discussed in Section 3, translational noise tends to suppress the swimmer's tactic shift, though not completely.

In Figure 1c,d, we consider a periodic sequence of pulses, namely $v(x, t) = v_0 \sin^2[(x - ut)\pi/L]$, and measure the resulting steady-state tactic drift $v_x = \lim_{t \rightarrow \infty} \langle \dot{x} \rangle$ of the swimmer. Again, we keep the particle parameters v_0 and D_ϕ fixed and vary the wave parameters L and u . In the absence of translational noise (Figure 1c), we see essentially the same effect as in the case of a single activation pulse: v_x is negative for $u \ll v_0$ and turns positive as u approaches v_0 , exhibiting a pronounced maximum at $u \simeq v_0$. However, the ratio between the maximum strength of the positive and negative tactic velocity, respectively, appears to be inverted (for a single pulse, the negative shift at low u is markedly larger than the positive shift at $u \simeq v_0$). In this regard, we remind that in Figure 1c, we plotted the net tactic drift, i.e., the speed defined as an average tactic shift divided by the relevant observation time. Since the large negative shift in Figure 1b occurs over a long time (the time needed by the swimmer to fully cross the Gaussian pulse is proportional to L/u), we expect the tactic drift velocity in Figure 1c to be less pronounced in the negative regime.

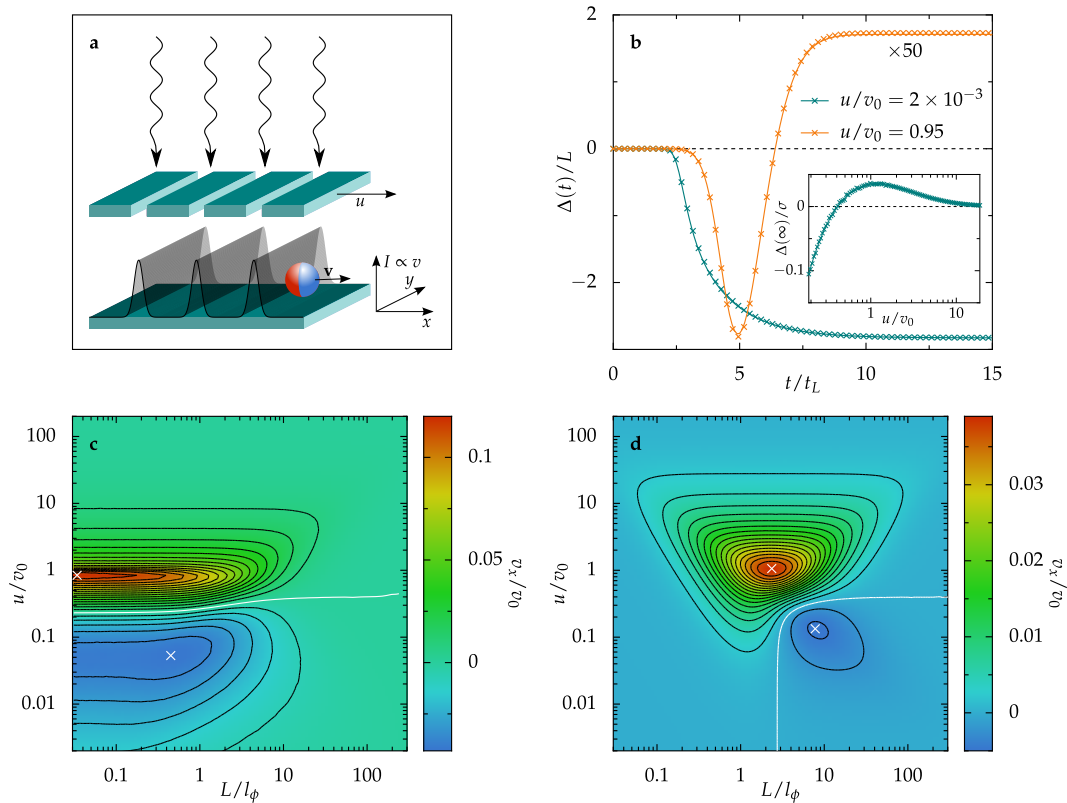


Figure 1. Taxis of an artificial microswimmer subjected to traveling activation pulses. (a) Model setup to experimentally realize activating wave pulses as considered in the present paper; see the text. (b) Tactic shift $\Delta(t)$ of the swimmer’s mean position generated by a Gaussian activation pulse, $v(x, t) = v_0 \exp[-(x - ut)^2/(2L^2)]$, vs. time t in units of the pulse crossing time $t_L = L/u$. In the inset, the final shift $\Delta(\infty)$ is plotted as a function of the pulse speed u . The swimmer’s self-propulsion parameters were set to $v_0 = 53 \mu\text{m/s}$ and $D_\phi = 165 \text{s}^{-1}$, and the pulse width was chosen according to $L = 1 \mu\text{m}$, about three times the swimmer’s propulsion length $l_\phi = v_0/D_\phi$. Here, the translational noise intensity D_0 was set to zero in order to focus on the essential mechanism giving rise to the swimmer’s tactic shift. (c,d) Tactic drift v_x induced by a sinusoidal activation pulse, $v(x, t) = v_0 \sin^2[(x - ut)\pi/L]$. The swimmer’s parameters are the same as in (b), and we set $D_0 = 0$ in (c) and $D_0 = 2.2 \mu\text{m}^2/\text{s}$ in (d). The position of the maximum positive drift and the maximum negative drift, respectively, is marked by white crosses, and the white contours depict the separatrices dividing the regions of positive and negative taxis. All results were obtained either by stochastic integration of the Langevin Equations (LEs) (1) ((b), crosses and (c)) or by solving the corresponding Fokker–Planck Equation (FPE) (3) ((b), solid lines and (d)); see [30] for numerical details.

Moreover, we note that for pulse wavelengths L larger than the swimmer’s persistence length l_ϕ , the action of the rotational noise becomes appreciable, leading to a suppression of v_x . This behavior is clearly consistent with Equation (3), where for $D_0 = 0$, an increase in L is equivalent to an increase in D_ϕ .

As illustrated in Figure 1d, translational fluctuations, $D_0 > 0$, suppress the tactic drift of the swimmer, as well, because they help it diffuse across the wave troughs in both directions. Furthermore, the particle’s “surfing” effect becomes less efficient, and the tactic speed, v_x , diminishes overall. However, we notice that the translational noise has a stronger impact for small values of L , where it drastically suppresses the negative drift. This causes a sharp down-bending of the separatrix curve that divides the regions of positive and negative taxis, in correspondence with a critical value of $D_0/(Lv_0)$ [30]. As a matter of fact, one sees immediately that a decrease in L is equivalent to an increase in D_0 , since it is easier for the translational noise to kick a swimmer out of a pulse of a smaller

width. By the same argument, it is also evident that translational fluctuations impact negative taxis more strongly than positive taxis. Indeed, the mechanism responsible for the negative drift requires preventing the swimmer from crossing a wave trough from left to right, which grows less efficient with increasing D_0 .

We furthermore stress that in Equation (1), we neglected hydrodynamic effects, which, at least in the absence of activation gradients, are strongly suppressed by: (i) restricting the swimmers' motion to the bulk, that is away from all confining walls; (ii) lowering the swimmer density so as to avoid particle clustering [37]; and (iii) choosing spherical active particles of a small size, i.e., almost point-like, in order to reduce hydrodynamic backflow effects. However, the modulated activation gradients considered here certainly give rise to additional hydrodynamic contributions, of which the most prominent one is a self-polarization of the swimmer: the particle strives to align itself parallel or anti-parallel to the gradient, depending on its surface properties [22,38]. We addressed the influence of such a self-polarizing torque on the swimmer's diffusion in a recent study [39] and concluded that for a small to moderate self-polarizing affinity, the tactic response of a swimmer behaves as reported in the present work. Its magnitude however slightly increases or decreases, subject to whether the swimmer tends to align itself parallel or anti-parallel to the gradient.

Finally, we remark that the setup considered in Figure 1a bears resemblance to that of [23]. However, a main difference between both setups is the way in which the spatial symmetry of the pulse waveform is broken, which was found to constitute the key factor, alongside the swimmer's finite persistence time, accountable for the emergence of any tactic drift. In the present setup, the pulse symmetry is broken due to the constant propagation of the pulses to the right, whereas in [23], an asymmetric pulse shape is considered. A tactic drift can be observed in both cases; however, the underlying mechanisms are rather different: in [23], the observed tactic effect is explained with a saturation of the self-polarizing torque mentioned above, while in the model as considered in the present work, the swimmer's tactic drift solely results from the modulation of its active diffusion inside the traveling wave pulses.

3. Results and Discussion

In the following, we analytically study the tactic drift of an artificial microswimmer subjected to traveling activation pulses. We assume that the spatio-temporal modulation of the swimmer's self-propulsion velocity has the form of a generic traveling wave, $v(x, t) = v_0 w[(x - ut)/L]$, with static profile $w(x/L)$. Upon changing coordinates from the resting laboratory frame to the co-moving wave frame, $x - ut \rightarrow x$, the Fokker–Planck equation (FPE) associated with the LEs (1) reads:

$$\frac{\partial P(\mathbf{r}, \phi, t)}{\partial t} = \left\{ D_0 \Delta - \nabla \left[v_0 w \left(\frac{x}{L} \right) \mathbf{n} - \mathbf{u} \right] + D_\phi \frac{\partial^2}{\partial \phi^2} \right\} P(\mathbf{r}, \phi, t), \quad (2)$$

where $\mathbf{r} = (x, y)^\top$, $\mathbf{u} = (u, 0)^\top$, $\mathbf{n} = (\cos \phi, \sin \phi)^\top$ and Δ and ∇ denote, respectively, the Laplace operator and the gradient in Cartesian coordinates (x, y) . The swimmer's dynamics perpendicular to the incoming wave exhibits no tactic behavior, since the pulse does not break the spatial symmetry in the y direction. Therefore, integrating over the y coordinate and conveniently rescaling x and t , $x =: Lx'$ and $t =: (L/v_0)t'$, we obtain a (still strictly Markovian) reduced FPE for the 2D marginal probability density $P(x', \phi, t')$, reading:

$$\frac{\partial P(x', \phi, t')}{\partial t'} = \left[\frac{D_0}{Lv_0} \frac{\partial^2}{\partial x'^2} - \frac{\partial}{\partial x'} \left(w(x') \cos \phi - \frac{u}{v_0} \right) + \frac{D_\phi L}{v_0} \frac{\partial^2}{\partial \phi^2} \right] P(x', \phi, t'). \quad (3)$$

Here, the effective rotational diffusion constant, $D_\phi L/v_0$, equals the ratio of the pulse width L to the swimmer's persistence length $l_\phi = v_0/D_\phi$. The effective translational diffusion constant, $D_0/(Lv_0)$, corresponds instead to the ratio of the time the swimmer takes to ballistically travel a pulse width L in a uniform activating medium, L/v_0 , to the time it takes to diffuse the same length subject to the sole

translational noise, L^2/D_0 . This ratio characterizes the relative strength of translational fluctuations and coincides with the reciprocal of the Péclet number for mass transport. We agree now to drop the prime signs, so that in the remaining sections, x and t denote the above dimensionless coordinates in the co-moving wave frame (unless stated otherwise).

3.1. Diffusive Regime

The wave pulses can be wide and slow enough to regard the swimmer’s motion inside each of them as purely diffusive. More precisely, this happens when the swimmer’s rotational diffusion time, D_ϕ^{-1} , is significantly smaller than the shortest ballistic pulse crossing time, $L/(v_0 + u)$, i.e., when $D_\phi L/v_0 \gg 1 + u/v_0$. Under this condition, we can further eliminate the orientational coordinate ϕ , so that the effects of self-propulsion boil down to an effective 1D diffusive dynamics. For this purpose, we apply to Equation (3) the homogenization mapping procedure detailed in [40] and obtain a partial differential equation for the marginal probability density:

$$\mathcal{P}(x, t) = \int_0^{2\pi} P(x, \phi, t) \, d\phi. \tag{4}$$

Following [41], we assume that the latter operation can be inverted by means of a “backward” operator $\hat{\psi}(x, \phi)$,

$$P(x, \phi, t) = \sum_{n=0}^{\infty} \epsilon^n \hat{\psi}_n(x, \phi) \frac{\mathcal{P}(x, t)}{2\pi}, \tag{5}$$

where $\hat{\psi}_0(x, \phi) = 1$ and $\epsilon := v_0/(D_\phi L)$. The expansion of $\hat{\psi}(x, \phi)$ in Equation (5) is justified by the fact that for $\epsilon \rightarrow 0$, the swimmer rotates infinitely quickly, in which case the self-propulsion can no longer contribute to its translational dynamics: the active particle behaves like a passive one, i.e., the rotational and translational dynamics decouple, and $P(x, \phi, t)$ simply becomes $\mathcal{P}(x, t)/(2\pi)$. Making use of Equations (4) and (5), respectively, in Equation (3) and reordering all terms thus obtained according to their powers of ϵ [40,41] yields a recurrence relation for the operators $\hat{\psi}_n$,

$$\begin{aligned} \partial_\phi^2 \hat{\psi}_{n+1}(x, \phi) &= \left[\hat{\psi}_n(x, \phi), \left(\frac{D_0}{Lv_0} \partial_x^2 + \frac{u}{v_0} \partial_x \right) \right] + \cos \phi \partial_x w(x) \hat{\psi}_n(x, \phi) \\ &\quad - \frac{1}{2\pi} \sum_{m=0}^n \hat{\psi}_{n-m}(x, \phi) \partial_x w(x) \int_0^{2\pi} \cos \phi \hat{\psi}_m(x, \phi) \, d\phi, \end{aligned} \tag{6}$$

where $[... , ...]$ denotes a commutator. By using the aforementioned initial condition $\hat{\psi}_0(x, \phi) = 1$, the periodicity condition $\hat{\psi}_n(x, 0) = \hat{\psi}_n(x, 2\pi)$ and the normalization condition $\int_0^{2\pi} \hat{\psi}_n(x, \phi) \, d\phi = 2\pi \delta_{n,0}$, Equation (6) can be solved iteratively, at least in principle, up to any arbitrarily high order. However, with increasing n , this task becomes more and more laborious, and the results for the $\hat{\psi}_n$ read increasingly complicated. In the diffusive limit, however, the swimmer’s rotational dynamics is significantly faster than its translational dynamics, and $P(x, \phi, t)$ relaxes very quickly in the ϕ direction, that is it only slightly differs from $\mathcal{P}(x, t)/(2\pi)$. It thus suffices to collect the terms of Equation (5) up to $\mathcal{O}(\epsilon)$, that is,

$$P(x, \phi, t) = \frac{1}{2\pi} [1 - \epsilon \cos \phi \partial_x w(x)] \mathcal{P}(x, t). \tag{7}$$

Finally, upon inserting Equation (7) into Equation (3) and successively integrating with respect to ϕ , we obtain the reduced 1D FPE [30]:

$$\frac{\partial \mathcal{P}(x, t)}{\partial t} = \hat{\mathbb{F}}(x) \mathcal{P}(x, t) = \left[\frac{\partial^2}{\partial x^2} \left(\frac{v_0}{2D_\phi L} w^2(x) + \frac{D_0}{Lv_0} \right) - \frac{\partial}{\partial x} \left(\frac{v_0}{4D_\phi L} \frac{dw^2(x)}{dx} - \frac{u}{v_0} \right) \right] \mathcal{P}(x, t), \tag{8}$$

which describes the probability density of the swimmer’s longitudinal position in the diffusive regime. Here, $\hat{\mathbb{F}}(x)$ denotes the Fokker–Planck operator, detailed on the right-hand side.

3.1.1. Single Activation Pulse

Following the presentation of Section 2, we first consider a single activating pulse hitting the swimmer and neglect translational fluctuations, $D_0 = 0$. The particle’s tactic shift is then obtained by measuring its displacement from an initial position x_0 , placed outside the pulse, on the right. Transforming back to the laboratory frame and taking the ensemble average, we define the tactic shift as $\Delta =: \langle x(t) \rangle - x_0 + ut/v_0$. Note that Δ is still expressed in terms of the dimensionless units introduced above. We now can quantify the tactic shift in two ways: we either set a time t and calculate the corresponding average swimmer’s displacement in the pulse frame, $\langle x(t) \rangle$, hence:

$$\Delta(t) = \langle x(t) \rangle - x_0 + \frac{u}{v_0}t, \tag{9}$$

or, vice versa, we set the longitudinal shift, $x_1 - x_0$, in the moving frame and calculate the corresponding mean first-passage time $\langle t(x_1|x_0) \rangle$, hence:

$$\tilde{\Delta}(x_1) = x_1 - x_0 + \frac{u}{v_0} \langle t(x_1|x_0) \rangle. \tag{10}$$

We remind that $\langle t(x_1|x_0) \rangle$ denotes the average time the particle takes to reach x_1 for the first time from x_0 [42].

As long as $x_1 < x_0$, both methods are valid and equivalent, since in the moving frame, the swimmer travels to the left and its position eventually takes on all values with $x < x_0$. However, for finite t and x_1 , we a priori do not know how to choose the values x_1 and t that verify the identity $\Delta(t) = \tilde{\Delta}(x_1)$. However, if we consider the full shift of the swimmer after it has completely crossed the pulse (that is, for large enough t or for x_1 placed far enough to the left of the pulse), both expressions yield the same result, that is, $\Delta(\infty) = \tilde{\Delta}(-\infty)$. This identity proved very helpful, since for the problem at hand, the mean first-passage time can be calculated in a much simpler way than the average particle position. If the Fokker–Planck operator is time independent, the mean first-passage time is the solution of the ordinary differential equation $\hat{\mathbb{F}}^\dagger(x) \langle t(x_1|x) \rangle = -1$ [43,44]. Here, $\hat{\mathbb{F}}^\dagger$ is the adjoint Fokker–Planck operator acting upon the swimmer’s starting position x , now taken as a variable, and $\langle t(x_1|x) \rangle$ obeys an absorbing boundary condition, $\langle t(x_1|x_1) \rangle = 0$, at $x = x_1$. We thus have to solve the ordinary differential equation:

$$-1 = \left[\frac{v_0}{2D_\phi L} w^2(x) \frac{\partial^2}{\partial x^2} + \left(\frac{v_0}{4D_\phi L} \frac{dw^2(x)}{dx} - \frac{u}{v_0} \right) \frac{\partial}{\partial x} \right] \langle t(x_1|x) \rangle. \tag{11}$$

A second boundary condition follows naturally from the observation that outside of the pulse, the swimmer’s motion is deterministic. Namely, we know that $\dot{x} = -u/v_0$ at $x = x_0$, hence:

$$\left. \frac{\partial \langle t(x_1|x) \rangle}{\partial x} \right|_{x=x_0} = \frac{v_0}{u} \tag{12}$$

(because the swimmer starts at a position with $x > x_1$, to the right of the pulse, and crosses it to the left, increasing x causes an increase in $\langle t(x_1|x) \rangle$). With the above boundary conditions, Equation (11) returns a unique solution,

$$\langle t(x_1|x) \rangle = \int_{x_1}^x \left[\frac{v_0}{u} \exp \left(\int_y^{x_0} f(q) dq \right) + \int_y^{x_0} \frac{2}{\epsilon w^2(z)} \exp \left(\int_y^z f(q) dq \right) dz \right] dy, \tag{13}$$

where $\epsilon = v_0/(D_\phi L)$ and:

$$f(q) := \left(\frac{\epsilon}{4} \frac{dw^2(q)}{dq} - \frac{u}{v_0} \right) \left(\frac{\epsilon}{2} w^2(q) \right)^{-1} = \frac{d \ln(q)}{dq} - \frac{2u}{\epsilon v_0 w^2(q)}. \tag{14}$$

For a smoothly decaying pulse profile $w(x)$, the condition for the swimmer to sweep through the entire pulse requires taking the limits $x_0 \rightarrow \infty$ and $x_1 \rightarrow -\infty$. The tactic shift of a swimmer in the diffusive regime is thus given by the expression:

$$\Delta(\infty) = \lim_{\substack{x_1 \rightarrow -\infty \\ x_0 \rightarrow \infty}} \left\{ x_1 - x_0 + \frac{u}{v_0} \int_{x_1}^{x_0} \left[\frac{v_0}{u} \exp \left(\int_y^{x_0} f(q) dq \right) + \int_y^{x_0} \frac{2}{\epsilon w^2(z)} \exp \left(\int_y^z f(q) dq \right) dz \right] dy \right\}. \tag{15}$$

The right-hand side of Equation (15) contains two removable singularities; a partial integration yields the more compact result:

$$\Delta(\infty) = \int_{-\infty}^{\infty} \frac{1}{w(y)} \int_y^{\infty} \frac{dw(z)}{dz} \exp \left(-2 \frac{D_\phi L}{v_0} \frac{u}{v_0} \int_y^z \frac{1}{w^2(q)} dq \right) dz dy. \tag{16}$$

Note that this expression is independent of the boundary condition (12). Indeed, outside the pulse, i.e., when $w(x) = 0$, Equation (11) reduces to a first-order differential equation, and thus, the boundary condition at $x = x_0$ becomes superfluous. A comparison between the analytical prediction of Equation (16) and results obtained by numerically integrating the FPE (3) is plotted in Figure 2. As in Section 2, for the activating pulse, we chose a Gaussian profile, $w(x) = \exp(-x^2/2)$, of width $L \sim 12l_\phi$ (we remark that due to the dimensionless scaling introduced at the beginning of this section, L does not explicitly enter the waveform anymore, but instead, it is incorporated into the effective diffusion constants; see Equation (3)). The analytical and numerical curves for $\Delta(\infty)$ versus u overlap in the regime of slow pulse speeds, $u \ll v_0$, thus confirming the validity of the diffusive approximation.

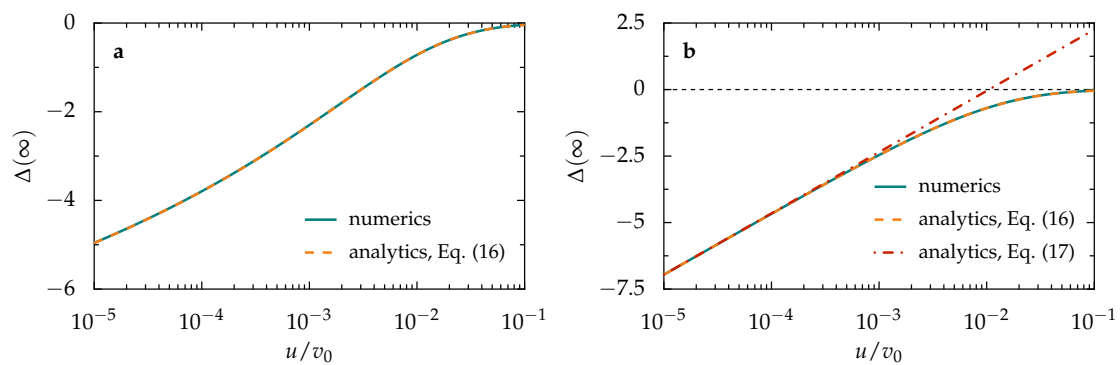


Figure 2. Tactic shift of an artificial microswimmer across a single traveling pulse of the form (a) $w(x) = \exp(-x^2/2)$ and (b) $w(x) = \text{sech}(x)$: $\Delta(\infty)$ vs. u in units of the self-propulsion speed, v_0 . The swimmer parameters are as in Figure 1b: $v_0 = 53 \mu\text{m/s}$, $D_\phi = 165 \text{ s}^{-1}$ and $D_0 = 0$. We remind that here x and $\Delta(\infty)$ are expressed in units of L . In (a), $L = 4 \mu\text{m}$, i.e., about 12 times l_ϕ ; in (b), L was set to $3.58 \mu\text{m}$, so that the two pulse profiles have the same half-width. The numerical results were obtained by solving the FPE (3).

Moreover, for a soliton-like pulse profile, that is $w(x) = \text{sech}(x)$, we succeeded in obtaining an explicit analytical expression for $\Delta(\infty)$, namely (see Appendix A):

$$\Delta(\infty) = \frac{\pi}{2} + \gamma - \ln \left(\frac{v_0}{D_\phi L} \frac{v_0}{u} \right), \tag{17}$$

where γ denotes the Euler–Mascheroni constant. Here, the agreement between numerical results and analytic approximation is quite close, as well. The range of validity of Equation (17), however, shrinks to lower values of u/v_0 , compared to the general result of Equation (16), which is due to the fact that in the derivation of Equation (17), we repeatedly assumed a very slow pulse propagation; see Equation (A2).

The analytical estimate of $\Delta(\infty)$ in Equation (17) lends itself to a simple heuristic interpretation. As mentioned in Section 2, in the diffusive regime, the effective pulse half-width, x_u , is defined by the identity $w(x_u) = u/v_0$. Since for $u \ll v_0$, the swimmer propels itself inside an almost static pulse until it exits for good to its left, its tactic shift must be of the order of x_u . For the soliton-like profile $w(x) = \text{sech}(x)$, this implies that:

$$\Delta(\infty) \approx -\ln\left(\frac{2v_0}{u}\right). \tag{18}$$

Of course, this argument cannot fully reproduce Equation (17). Nevertheless, it explains why the swimmer’s tactic shift diverges in the limit $u \rightarrow 0$: as the pulse nearly comes to rest, its effective width grows exceedingly large; in the diffusive regime, the effect of the pulse’s fore-rear symmetry breaking is therefore steadily enhanced.

Analogously, for the slow Gaussian pulse of Figures 1b and 2a, the dependence of $\Delta(\infty)$ on u is expected to be of the form $\sqrt{2\ln(v_0/u)}$, also in good agreement with our numerical and analytical curves. Here, the pulse tails decay more quickly than for the soliton-like pulse, thus leading to a smaller tactic shift in the limit $u \rightarrow 0$.

The influence of translational noise: We next consider the more realistic case with non-zero translational fluctuations, $D_0 > 0$. A very low translational noise level may be negligible in an appropriate range of pulse speeds. However, for $u \rightarrow 0$, the timescale on which the tactic shift approaches its asymptotic value, $\Delta(\infty)$, grows exceedingly long, which implies that at least in this regime, translational fluctuations must be taken into account. To a good approximation, the translational noise strength is independent of the spatio-temporal modulation of the swimmer’s activation mechanism (see Equation (1)). As a main difference with the noiseless case $D_0 = 0$, in the presence of translational noise, the pulse edges are “open”, as the swimmer can now cross them repeatedly back and forth. However, for sufficiently long observation times, the swimmer surely moves past the pulse, no matter how small u and large D_0 . Therefore, for $D_0 > 0$, we can calculate $\Delta(\infty)$ following the procedure already adopted for $D_0 = 0$. Even the boundary condition (12) remains unchanged (and here is not superfluous), since at $x = x_0$, that is outside the pulse, we have $\langle \dot{x} \rangle = -u/v_0$. We thus obtain:

$$\Delta(\infty) = \int_{-\infty}^{\infty} \int_y^{\infty} \frac{w(z) \frac{dw(z)}{dz}}{\sqrt{[w^2(y) + \alpha][w^2(z) + \alpha]}} \exp\left(-2\frac{D_\phi L}{v_0} \frac{u}{v_0} \int_y^z \frac{1}{w^2(q) + \alpha} dq\right) dz dy, \tag{19}$$

with $\alpha := 2D_0D_\phi/v_0^2$. Obviously, in the limit $D_0 \rightarrow 0$, we recover Equation (16).

In Figure 3, the dependence of $\Delta(\infty)$ on the pulse speed u was determined both by computing the integrals in Equation (19) and numerically solving Equation (3). Again, the agreement between analytical and numerical results is quite close. We notice that in the presence of translational noise, the limit of $\Delta(\infty)$ for $u \rightarrow 0$ is finite. We attribute this property to the fact that translational diffusion, which tends to suppress tactic rectification, prevails over self-propulsion, but only in the pulse’s tails. More precisely, the swimmer’s dynamics is dominated by translational diffusion when $D_0/(Lv_0) \gg v_0w^2(x)/(2D_\phi L)$ (see Equation (8)) or $w^2(x) \ll \alpha$ (see Equation (19)). Under this condition, a natural definition of the effective pulse width is $\min[x_u, x_t]$, with x_t being the solution of the equation $w(x_t) \propto \sqrt{2D_0D_\phi/v_0^2}$. On decreasing u , the ratio x_u/x_t diverges, the effective pulse width coincides with x_t and $\Delta(\infty)$ becomes a function of the sole parameter $\alpha = 2D_0D_\phi/v_0^2$.

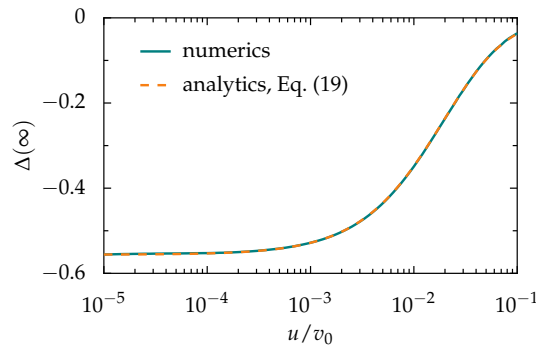


Figure 3. Tactic shift $\Delta(\infty)$ as in Figure 2a, but for non-zero translational noise with $D_0 = 2.2 \mu\text{m}^2/\text{s}$. The numerical results were again obtained by solving the FPE (3).

3.1.2. Periodic Pulse Train

In the following, we consider a periodic sequence of activating pulses, $w(x + n) = w(x) \forall n \in \mathbb{Z}$, with unit period (in dimensionless units), which corresponds to a period of L in the unscaled notation of Section 2. To calculate the resulting longitudinal drift speed, $v_x = \lim_{t \rightarrow \infty} \langle \dot{x} \rangle + u/v_0$ from Equation (8), we introduce the reduced one-zone probability:

$$\tilde{\mathcal{P}}(x, t) = \sum_{n=-\infty}^{\infty} \mathcal{P}(x + n, t), \tag{20}$$

which maps the overall probability density $\mathcal{P}(x, t)$ onto one period of the pulse sequence [30,45,46]. That is, instead of considering the time-evolution of the swimmer’s probability density along an infinite periodic pulse sequence, we focus on a single wave period and impose periodic boundary conditions to ensure the existence of a stationary state. Accordingly, we define the corresponding reduced probability current, $\tilde{J}(x, t)$, and obtain the continuity equation:

$$\frac{\partial \tilde{\mathcal{P}}(x, t)}{\partial t} = -\frac{\partial \tilde{J}(x, t)}{\partial x}, \tag{21}$$

where, upon introducing the two auxiliary functions $g(x) := v_0 w^2(x)/(2D_\phi L) + D_0/(Lv_0)$ and $h(x) := v_0(d/dx)w^2(x)/(4D_\phi L) - u/v_0$, $\tilde{J}(x, t)$ can be written in a compact form as:

$$\tilde{J}(x, t) = -\exp\left(\int_0^x \frac{h(y)}{g(y)} dy\right) \frac{\partial}{\partial x} g(x) \exp\left(-\int_0^x \frac{h(y)}{g(y)} dy\right) \tilde{\mathcal{P}}(x, t). \tag{22}$$

In the stationary limit, $\tilde{J}(x, t \rightarrow \infty) =: \tilde{J}_{\text{st}}$ becomes constant and can be calculated explicitly [46],

$$\begin{aligned} \tilde{J}_{\text{st}} &= \frac{v_0}{2D_\phi L} \left[1 - \exp\left(2\frac{D_\phi L}{v_0} \frac{u}{v_0} \int_0^1 \frac{1}{w^2(x) + \alpha} dx\right) \right] \\ &\times \left[\int_0^1 \int_0^1 \frac{1}{\sqrt{[w^2(x) + \alpha][w^2(x+y) + \alpha]}} \exp\left(2\frac{D_\phi L}{v_0} \frac{u}{v_0} \int_x^{x+y} \frac{1}{w^2(z) + \alpha} dz\right) dy dx \right]^{-1}. \end{aligned} \tag{23}$$

Upon transforming back to the laboratory frame, we finally obtain a simple expression for the swimmer’s tactic drift speed, namely:

$$v_x = \int_0^1 \tilde{J}_{\text{st}} dx + \frac{u}{v_0} = \tilde{J}_{\text{st}} + \frac{u}{v_0}. \tag{24}$$

Taking the limit $D_0 \rightarrow 0$ and assuming $w(0) = w(1) = 0$ (as for $w(x) = \sin^2(\pi x)$ in Figure 1c,d), Equation (23) can be given the more convenient form:

$$\tilde{J}_{st} = \frac{u}{v_0} \left[\int_0^1 \int_0^1 \frac{w'(x+y)}{w(x)} \exp \left(-2 \frac{D_\phi L}{v_0} \frac{u}{v_0} \int_{x+y}^{x+1} \frac{1}{w^2(z)} dz \right) dy dx \right]^{-1}, \quad (25)$$

where the prime sign denotes the derivative with respect to the function's argument.

In Figure 4, we compare the analytical approximation of Equations (23)–(25) with the exact values for v_x , computed by numerically integrating the FPE (3) or the LEs (1). As for that, we remark that both numerical approaches yield, within their accuracy, the same results, so that we can adopt either of them, as more convenient. In general, solving the FPE is advantageous, since numerically integrating the LEs for an ensemble of particles is rather time consuming. For some parameter ranges, however, namely when the probability density $P(x, \phi, t)$ is sharply peaked, the spatial grid, on which the temporal evolution of the FPE is solved, has to be extremely fine. Memory consumption and computation time then explode, so that numerically integrating the LEs proves more effective.

As expected, a close agreement between the numerical and analytical curves in Figure 4 is achieved if both conditions $D_\phi L/v_0 \gg 1$ and $u/v_0 \ll 1$ are simultaneously fulfilled. In contrast to our initial conjecture, under the weaker condition $D_\phi L/v_0 \gg 1 + u/v_0$, the motion of an active swimmer inside a traveling pulse may well be regarded as purely diffusive, but the corresponding diffusive approximation fails to correctly predict its tactic drift when $u \gtrsim v_0$ (see Figure 4b,d).

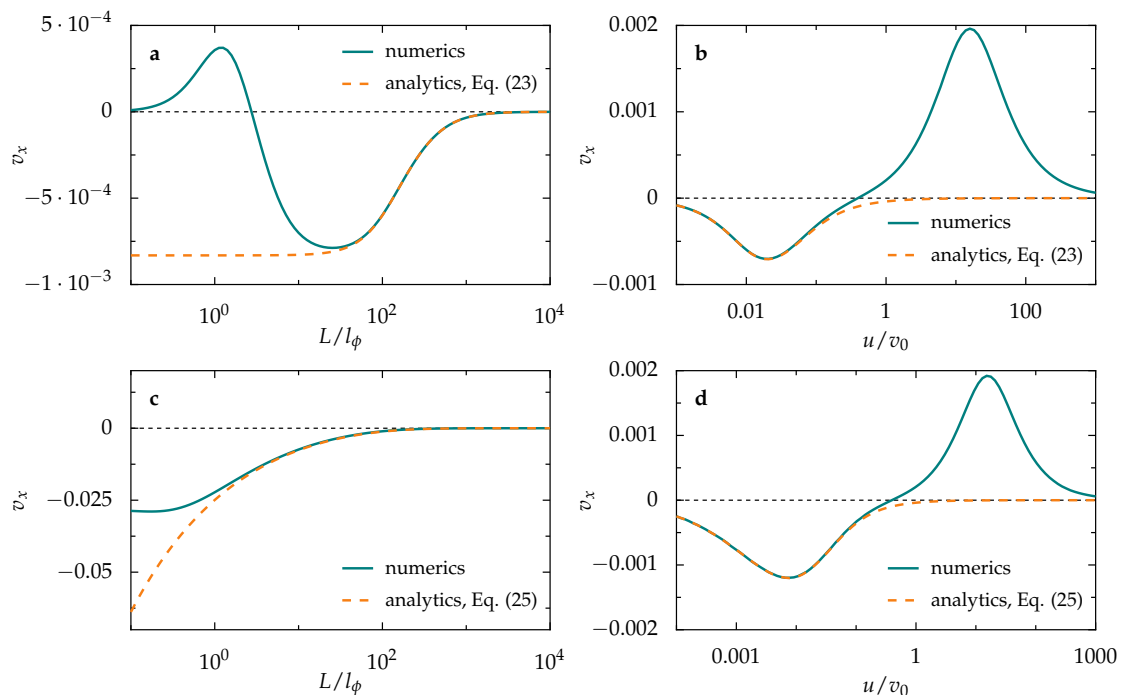


Figure 4. Tactic drift velocity of an artificial microswimmer subjected to the sinusoidal activating pulse sequence of Figure 1c,d: v_x vs. the pulse width L (a,c) and pulse speed u (b,d). The swimmer parameters v_0 and D_ϕ are the same as in the previous figures and $D_0 = 2.2 \mu\text{m}^2/\text{s}$ in (a,b) ($D_0 = 0$ in (c,d)). Furthermore, $u = 0.01v_0$ in (a,c) and $L = 100l_\phi$ in (b,d). The numerical data plotted here have been obtained by numerically integrating the LEs (1) or, equivalently, the FPE (3).

As a consequence, we find that the positive branches of the v_x curves are purely determined by the ballistic nature of the swimmer's dynamics (which is indeed rather subordinate for $L \gg l_\phi$, but nevertheless cannot be neglected if $u \gtrsim v_0$). This conclusion is supported by Figure 4a,c, where

for $L/l_\phi \lesssim 10$, the tactic response clearly depends on D_0 , and more importantly, the analytic and numerical curves seem to part ways. In the diffusive approximation (dashed curves), the effect of the translational fluctuations is predicted to just prevent the drift from growing more negative, whereas in the full dynamics treatment (solid curves), the influence of D_0 causes v_x to change sign.

3.2. Ballistic Regime

We focus now on the opposite dynamical regime, termed ballistic. Here, the traveling pulses are assumed to be so narrow and sweep through the swimmer so quickly that the swimmer’s orientation almost does not change during a single pulse crossing, i.e., the time a single activating pulse takes to pass the swimmer is negligible with respect to the angular diffusion time D_ϕ^{-1} . In such a limit, we take ϕ constant and rewrite the FPE (3) as:

$$\frac{\partial P_\phi(x, t)}{\partial t} = \left[\frac{D_0}{Lv_0} \frac{\partial^2}{\partial x^2} - \frac{\partial}{\partial x} \left(w(x) \cos \phi - \frac{u}{v_0} \right) \right] P_\phi(x, t), \tag{26}$$

where $P_\phi(x, t)$ is the corresponding conditional probability density at fixed angle ϕ . In the following, we make use of Equation (26) to calculate the conditional tactic shift, $\Delta_\phi(\infty)$, or drift, v_x^ϕ , as appropriate. Since the angular coordinate is actually not fixed, but rather freely diffusing on an exceedingly long timescale, the quantities $\Delta_\phi(\infty)$ and v_x^ϕ will be eventually averaged with respect to ϕ , which is uniformly distributed on the interval $[0, 2\pi]$.

3.2.1. Single Activation Pulse

The tactic shift $\Delta(\infty)$ of a swimmer swept through a single activating pulse can be calculated, once again, as in Section 3.1.1, namely:

$$\Delta(\infty) = \frac{1}{2\pi} \int_0^{2\pi} \Delta_\phi(\infty) d\phi = \frac{Lv_0}{D_0} \int_{-\infty}^{\infty} \int_x^{\infty} w(y) \exp \left[-\frac{Lu}{D_0}(y-x) \right] I_1 \left(\frac{Lv_0}{D_0} \int_x^y w(z) dz \right) dy dx, \tag{27}$$

where $I_1(x) := (1/\pi) \int_0^\pi \exp(x \cos \phi) \cos \phi d\phi$ is a modified Bessel function of the first kind [47]. Although in the absence of translational fluctuations, $D_0 = 0$, the swimmer’s fixed-angle dynamics is purely deterministic, we can still employ the mean first-passage time technique to calculate $\Delta(\infty)$ for $D_0 = 0$, yielding:

$$\Delta(\infty) = \int_{-\infty}^{\infty} \left(\frac{1}{\sqrt{1 - (v_0^2/u^2) w^2(x)}} - 1 \right) dx, \tag{28}$$

which surely is well-defined in the ballistic regime with $u > v_0$. Here, the positive tactic shift must be attributed to the fact that swimmers oriented to the right, i.e., parallel to the direction of pulse propagation, “surf” the pulse for a longer time than swimmers oriented in the opposite direction.

By inspecting Figure 5, we notice that the ballistic approximation holds good for fast activating pulses. One might expect it to work well only if the swimmer’s rotational diffusion time, D_ϕ^{-1} , is larger than the timescale on which a swimmer oriented to the right ($\phi = 0$) ballistically crosses the pulse, $L/(u - v_0)$. By analogy with Section 3.1, one would end up with the condition $u/v_0 \gg 1 + L/l_\phi$. This argument however totally disregards the influence of translational fluctuations and thus only applies when $D_0/(Lv_0)$ can be safely neglected (see Figure 5a). More in general, we must require that D_ϕ^{-1} is larger than the pulse crossing timescale in the ballistic regime, $L/(u - v_0)$, or in the diffusive regime, L^2/D_0 , whichever is smaller. This leads to the weaker condition for the validity of the ballistic approximation, $l_\phi/L \gg \min [(u/v_0 - 1)^{-1}, Lv_0/D_0]$.

By comparing the data for $D_0 = 0$ and $D_0 > 0$ in Figure 5, we also observe that translational fluctuations affect the tactic response of a ballistic swimmer only marginally: contrary to the diffusive regime, here, the swimmer crosses the pulse quite quickly, so that the translational noise has almost

no time to act on it (provided the pulses are not too narrow). The simple expression of Equation (28) can thus be safely employed to predict the tactic shift of a swimmer in the ballistic regime also in the presence of translational noise.

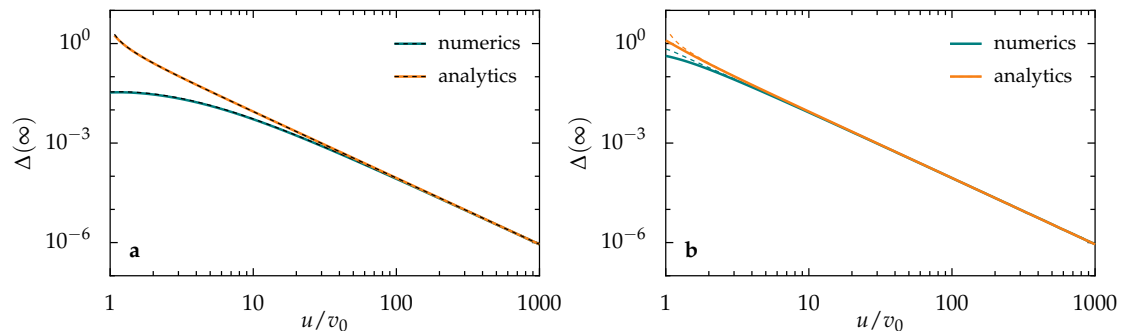


Figure 5. Tactic shift of an artificial microswimmer hit by a single Gaussian pulse, like in Figures 2 and 3, but for larger values of the pulse speed u . The particle parameters are as in the previous figures; furthermore, $L = 1 \mu\text{m}$ ($\sim 3l_\phi$) in (a) and $0.1 \mu\text{m}$ in (b). The numerical curves were obtained by solving the FPE (3) or integrating the LEs (1); the analytical curves were calculated in the ballistic approximation of Equation (27) or (28), as appropriate. For the sake of a comparison, we plotted the curves for $D_0 = 2.2 \mu\text{m}^2/\text{s}$ (solid lines) together with the corresponding curves for $D_0 = 0$ (dashed lines).

3.2.2. Periodic Pulse Train

For the periodic sequence of activation pulses introduced in Section 3.1.2, the swimmer’s tactic drift can also easily be calculated in the ballistic approximation, and we obtain analogously as in Section 3.1.2:

$$v_x = \frac{D_0}{2\pi L v_0} \int_0^{2\pi} \left\{ 1 - \exp \left[\frac{L v_0}{D_0} \left(\frac{u}{v_0} - \cos \phi \int_0^1 w(x) dx \right) \right] \right\} \times \left\{ \int_0^1 \int_0^1 \exp \left[\frac{L v_0}{D_0} \left(\frac{u}{v_0} y - \cos \phi \int_x^{x+y} w(z) dz \right) \right] dy dx \right\}^{-1} d\phi + \frac{u}{v_0}. \quad (29)$$

If we further neglect translational fluctuations, $D_0 = 0$, in the ballistic regime, the longitudinal LE (1) simplifies to a purely deterministic fixed-angle equation of motion, $\dot{x} = w(x) \cos \phi - u/v_0$. For a sinusoidal pulse sequence, $w(x) = \sin^2(\pi x)$, this equation can be solved analytically, i.e.,

$$x(t) = \begin{cases} -\frac{1}{\pi} \arctan \left[\frac{\tan(\pi t u/v_0 \sqrt{1-(v_0/u) \cos \phi})}{\sqrt{1-(v_0/u) \cos \phi}} \right] & : t \leq \frac{v_0}{2u \sqrt{1-(v_0/u) \cos \phi}} \\ -\frac{1}{\pi} \arctan \left[\frac{\tan(\pi t u/v_0 \sqrt{1-(v_0/u) \cos \phi})}{\sqrt{1-(v_0/u) \cos \phi}} \right] - 1 & : t > \frac{v_0}{2u \sqrt{1-(v_0/u) \cos \phi}}, \end{cases} \quad (30)$$

with x restricted to the interval $[-1, 0]$, $u > v_0$, and initial condition $x(0) = 0$. The ballistic pulse crossing time t_c^ϕ for a fixed orientation angle, defined by the relation $x(t_c^\phi) = -1$, thus reads $t_c^\phi = v_0 / (u \sqrt{1 - (v_0/u) \cos \phi})$. The swimmer’s tactic drift can then be calculated using the known relation $v_x^\phi = -1/t_c^\phi + u/v_0$. If u grows smaller than v_0 , however, particles oriented to the right can get trapped inside the pulses. This occurs when their self-propulsion speed in the x direction, $v_0 w(x) \cos \phi$, compensates for the translational speed, $-u$. As $w(x)$ is valued between zero and one,

swimmers get trapped with orientation $-\arccos(u/v_0) < \phi < \arccos(u/v_0)$. In the co-moving pulse frame, the velocity of trapped swimmers is zero, so that the ϕ -averaged drift velocity turns out to be:

$$v_x = \begin{cases} -\frac{u}{v_0} \left(\frac{1}{2\pi} \int_0^{2\pi} \sqrt{1 - \frac{v_0}{u} \cos \phi} d\phi - 1 \right) & : \frac{u}{v_0} \geq 1 \\ -\frac{u}{v_0} \left(\frac{1}{2\pi} \int_{\arccos(u/v_0)}^{2\pi - \arccos(u/v_0)} \sqrt{1 - \frac{v_0}{u} \cos \phi} d\phi - 1 \right) & : \frac{u}{v_0} < 1. \end{cases} \quad (31)$$

It is interesting to remark that we can now refine the validity criterion for the ballistic approximation discussed in the previous section, owing to the more precise estimate of the ballistic pulse-crossing time derived above. Following the relevant argument of Section 3.2.1, we thus expect the ballistic approximation to hold for $l_\phi/L > \min(t_c^{\phi=0}, Lv_0/D_0)$.

A comparison between exact numerics and the ballistic approximation is shown in Figure 6. As expected, its range of validity in the parameter u shrinks on increasing L/l_ϕ , and the refined validity condition just introduced provides an estimate of that range. Another interesting property illustrated in Figure 6 is that the ballistic approximation also predicts a regime of negative tactic drift, which we explain as follows. We have already mentioned that for $u > v_0$, all swimmers surely cross the wave pulse, and the positive net drift results from the fact that particles oriented parallel to the direction of pulse propagation spend on average a longer time inside the pulse than particles oriented in the opposite direction. For $u < v_0$, however, the emerging trapping mechanism causes swimmers with $-\arccos(u/v_0) < \phi < \arccos(u/v_0)$ to travel to the right with velocity u . If u is suitably smaller than v_0 , the trapped swimmers may happen to move considerably slower to the right than swimmers with $|\phi| > \pi/2$ to the left, thus causing a negative net drift.

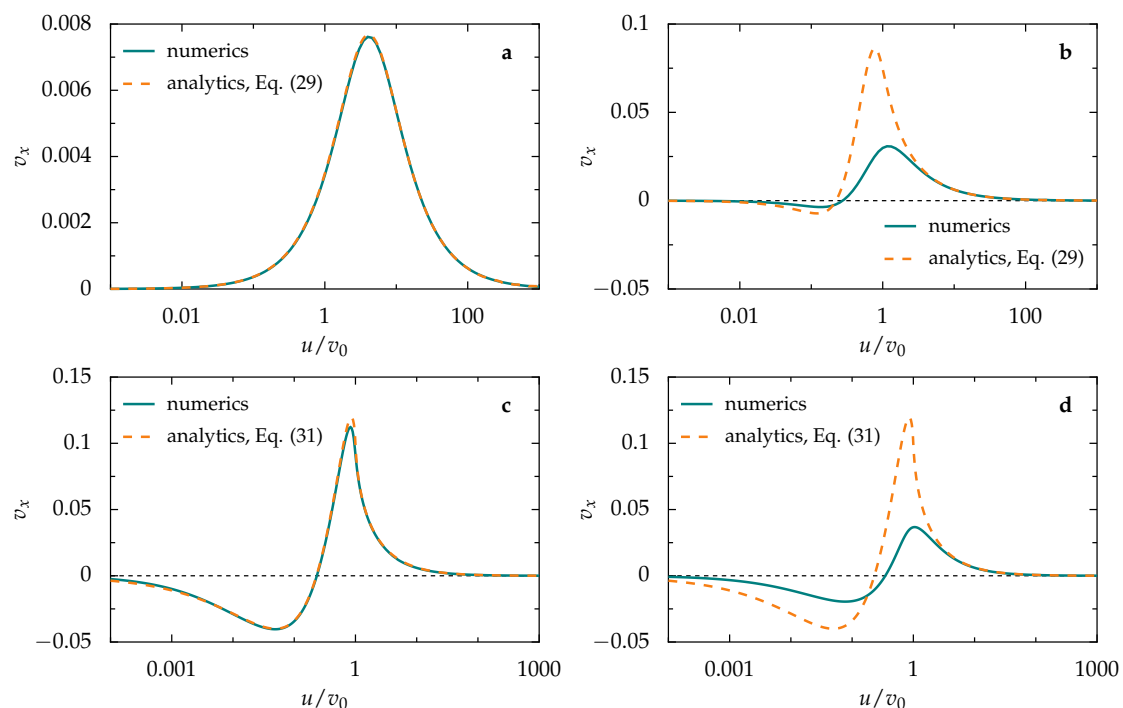


Figure 6. Tactic drift of an artificial microswimmer induced by the sinusoidal pulse sequence of Figure 4: v_x vs. u in units of v_0 . In (a,c), we chose a very small pulse periodicity, $L = 0.2l_\phi$, whereas in (b,d), L was set to $5l_\phi$. The swimmer parameters v_0 and D_ϕ were chosen as in the previous figures and we set $D_0 = 2.2 \mu\text{m}^2/\text{s}$ in (a,b) and $D_0 = 0$ in (c,d). The numerical curves were obtained by numerically integrating the LEs (1) or solving the FPE (3).

4. Conclusions

In summary, we analytically showed that the dynamics of artificial microswimmers subjected to traveling activation pulses manifests two, partially competing tactic effects, both induced by the broken spatial symmetry associated with the pulse propagation. In the two limiting regimes of high and low rotational fluctuations, defined with respect to the pulse parameters u and L , we obtained analytical approximations that are in close agreement with the exact numerical results. Likewise, these analytical results compare favorably with the numerical data reported before in [30]. Our analytical approach provides a valuable framework for future studies of the tactic response of artificial microswimmers in spatio-temporally modulated activation media. Moreover, we identified the positive tactic drift as being a purely ballistic effect, i.e., to stem solely from the finite persistence of the swimmer's active Brownian motion, whereas the negative tactic drift results from the combination of diffusive and ballistic properties of the swimmer's dynamics.

A generalization of the single particle model considered in the present work to multiple interacting swimmers, slightly similar to the setup considered in [48] for macroscopic phototactic robots, could also give rise to interesting new collective effects, primarily stemming from the coupling of the hydrodynamic swimmer interactions to the hydrodynamic influence of the activation gradient [39].

Acknowledgments: This work has been supported by the cluster of excellence Nanosystems Initiative Munich (Peter Hänggi). Peter Hänggi and Fabio Marchesoni acknowledge financial support from the Augsburg Centre for Innovative Technology (ACIT) of the University of Augsburg. Fabio Marchesoni also thanks the German Academic Exchange Service (DAAD) for a Visiting Professor grant.

Author Contributions: Alexander Geiseler performed all calculations in this project. All authors contributed to the planning and the discussion of the results, as well as to the writing of this work.

Conflicts of Interest: The authors declare no conflict of interest.

Appendix A. Tactic Shift Induced by a Soliton-Like Pulse

Let the activating pulse have a simple exponentially decaying profile, $w(x) = \text{sech}(x)$, and $D_0 = 0$. Starting from Equation (8), we further rescale the time, $t = (v_0/u)\tau$, which leaves only one effective parameter, $\eta := v_0^2/(2D_\phi Lu)$, in the resulting FPE. Upon introducing the auxiliary coordinate χ , $x = \text{arsinh}(\sqrt{\eta}\chi)$, we rewrite the new FPE as:

$$\frac{\partial \mathcal{P}(\chi, \tau)}{\partial \tau} = \left(\frac{\partial^2}{\partial \chi^2} + \frac{\partial}{\partial \chi} \sqrt{\frac{1}{\eta} + \chi^2} \right) \mathcal{P}(\chi, \tau), \quad (\text{A1})$$

which, for slow wave pulses, $u \ll v_0^2/(2D_\phi L)$ or $\eta \gg 1$, respectively, can be approximated by:

$$\frac{\partial \mathcal{P}(\chi, \tau)}{\partial \tau} = \left(\frac{\partial^2}{\partial \chi^2} + \frac{\partial}{\partial \chi} |\chi| \right) \mathcal{P}(\chi, \tau). \quad (\text{A2})$$

For $\chi \geq 0$ [$\chi < 0$], the corresponding Fokker–Planck operator is associated with a Hermitian operator, $\hat{\mathbb{F}}(\chi) \rightarrow \exp(\chi^2/4)\hat{\mathbb{F}}(\chi)\exp(-\chi^2/4)$ [$\hat{\mathbb{F}}(\chi) \rightarrow \exp(-\chi^2/4)\hat{\mathbb{F}}(\chi)\exp(\chi^2/4)$] [44]. Accordingly, the FPE (A2) can be mapped onto the Schrödinger equation for a particle in the piecewise harmonic potential:

$$V(\chi) = \begin{cases} \frac{1}{4}(\chi^2 - 2) & : \chi \geq 0 \\ \frac{1}{4}(\chi^2 + 2) & : \chi < 0. \end{cases}$$

In principle, the probability density $\mathcal{P}(\chi, \tau)$ could be expressed in terms of the eigenvalues and eigenfunctions of such a Schrödinger equation, but in view of the potential cusp at $\chi = 0$, that would

be a challenging task. Therefore, we again resort to computing the mean first-passage time, $\langle \tau(\chi_1|\chi) \rangle$, by solving the relevant differential equation associated with the FPE (A2), namely:

$$-1 = \left(\frac{\partial^2}{\partial \chi^2} - |\chi| \frac{\partial}{\partial \chi} \right) \langle \tau(\chi_1|\chi) \rangle, \tag{A3}$$

with the boundary and continuity conditions:

- (i) $\langle \tau(\chi_1|\chi_1) \rangle = 0,$
- (ii) $\langle \tau(\chi_1|0^+) \rangle = \langle \tau(\chi_1|0^-) \rangle,$
- (iii) $\left. \frac{\partial \langle \tau(\chi_1|\chi) \rangle}{\partial \chi} \right|_{\chi=0^+} = \left. \frac{\partial \langle \tau(\chi_1|\chi) \rangle}{\partial \chi} \right|_{\chi=0^-},$
- (iv) $\left. \frac{\partial \langle \tau(\chi_1|\chi) \rangle}{\partial \chi} \right|_{\chi \rightarrow \infty} = 0.$

Its solution for $\chi \geq 0$ reads:

$$\langle \tau(\chi_1|\chi) \rangle = \frac{\pi}{2} \left[\operatorname{erfi} \left(\frac{\chi}{\sqrt{2}} \right) - \operatorname{erf} \left(\frac{\chi_1}{\sqrt{2}} \right) \right] - \frac{\chi^2}{2} {}_2F_2 \left(1, 1; \frac{3}{2}, 2; \frac{\chi^2}{2} \right) + \frac{\chi_1^2}{2} {}_2F_2 \left(1, 1; \frac{3}{2}, 2; -\frac{\chi_1^2}{2} \right), \tag{A4}$$

where $\operatorname{erfi}(x) = 2/\sqrt{\pi} \int_0^x \exp(v^2) dv$ is the imaginary error function and:

$${}_2F_2 \left(1, 1; \frac{3}{2}, 2; x \right) = \frac{\sqrt{\pi}}{x} \int_0^{\sqrt{x}} \operatorname{erf}(v) \exp(v^2) dv \tag{A5}$$

is a generalized hypergeometric function [49]. The swimmer’s tactic shift can now be formally computed as:

$$\Delta(\infty) = \lim_{\substack{x_1 \rightarrow -\infty \\ x_0 \rightarrow \infty}} \left\{ x_1 - x_0 + \frac{\pi}{2} \left[\operatorname{erfi} \left(\frac{\sinh(x_0)}{\sqrt{2\eta}} \right) - \operatorname{erf} \left(\frac{\sinh(x_1)}{\sqrt{2\eta}} \right) \right] - \frac{\sinh^2(x_0)}{2\eta} {}_2F_2 \left(1, 1; \frac{3}{2}, 2; \frac{\sinh^2(x_0)}{2\eta} \right) + \frac{\sinh^2(x_1)}{2\eta} {}_2F_2 \left(1, 1; \frac{3}{2}, 2; -\frac{\sinh^2(x_1)}{2\eta} \right) \right\}. \tag{A6}$$

(We remind that in the present notation the particle displacement in the laboratory frame is calculated as $x(t) - x_0 + \tau$.) To explicitly take the above limits, one must determine the asymptotic expansions of the special functions in Equation (A6). For $\operatorname{erfi}(x)$, this can be easily accomplished [50],

$$\operatorname{erfi}(x) \sim \frac{\exp(x^2)}{\sqrt{\pi} x}. \tag{A7}$$

The expansion of the hypergeometric function ${}_2F_2$ for $x \rightarrow \pm\infty$ is somewhat more elaborate. We start by considering its integral representation for negative arguments,

$${}_2F_2 \left(1, 1; \frac{3}{2}, 2; -x \right) = \frac{\sqrt{\pi}}{x} \int_0^{\sqrt{x}} \operatorname{erfi}(v) \exp(-v^2) dv \quad (x > 0), \tag{A8}$$

which follows directly from Equation (A5). By means of some algebraic substitutions and a binomial series expansion, the latter expression can then be brought to the form:

$${}_2F_2 \left(1, 1; \frac{3}{2}, 2; -x \right) = \frac{1}{2x} \int_0^x \frac{1 - \exp(-v)}{v\sqrt{1-v/x}} dv = \frac{1}{2} \sum_{m=0}^{\infty} \binom{-1/2}{m} (-1)^m x^{-(m+1)} \int_0^x v^{m-1} [1 - \exp(-v)] dv. \tag{A9}$$

The last integral in the above equation for $m = 0$ yields:

$$\int_0^x \frac{1 - \exp(-v)}{v} dv = \lim_{y \rightarrow 0} [\ln(x) - \ln(y) + E_1(x) - E_1(y)], \tag{A10}$$

where $E_1(x) = \int_x^\infty e^{-v}/v dv$ is the exponential integral [47]. Upon taking the leading orders of the limits $y \rightarrow 0$ and $x \rightarrow \infty$ of this expression, we finally obtain:

$$\int_0^x \frac{1 - \exp(-v)}{v} dv \sim \gamma + \ln(x), \tag{A11}$$

with $\gamma \approx 0.577$ denoting the Euler–Mascheroni constant. For $m \geq 1$, the integrand on the right-hand side of Equation (A9) can readily be integrated [51], namely:

$$\int_0^x v^{m-1} [1 - \exp(-v)] dv = \frac{x^m}{m} + \exp(-x) \sum_{k=0}^{m-1} \binom{m-1}{k} k! x^{m-1-k} \quad (m \geq 1). \tag{A12}$$

In conclusion, the asymptotic expansion of the hypergeometric function of Equation (A8) for large negative arguments reads, to the lowest orders,

$${}_2F_2\left(1, 1; \frac{3}{2}, 2; -x\right) \sim \frac{1}{2x} \left[\ln(x) + \gamma + \sum_{m=1}^{\infty} \binom{-\frac{1}{2}}{m} \frac{(-1)^m}{m} \right]. \tag{A13}$$

To sum the series of Equation (A13), we start from the integral representation of the digamma function $\psi(x)$ [51],

$$\psi(x) = -\gamma + \int_0^1 \frac{v^{x-1} - 1}{v - 1} dv, \tag{A14}$$

which, in turn, can be expanded in a binomial series, yielding:

$$\psi(x) = -\gamma - \sum_{m=1}^{\infty} \binom{x-1}{m} \frac{(-1)^m}{m}. \tag{A15}$$

On setting $x = 1/2$ in Equation (A15), one obtains the identity [47]:

$$\sum_{m=1}^{\infty} \binom{-\frac{1}{2}}{m} \frac{(-1)^m}{m} = -\gamma - \psi\left(\frac{1}{2}\right) = \ln(4), \tag{A16}$$

which, replaced into Equation (A13), leads to our final result,

$${}_2F_2\left(1, 1; \frac{3}{2}, 2; -x\right) \sim \frac{\ln(4x) + \gamma}{2x} \quad (x \rightarrow \infty). \tag{A17}$$

The asymptotic expansion of the ${}_2F_2$ function for large positive arguments follows immediately from the identity:

$${}_2F_2\left(1, 1; \frac{3}{2}, 2; x\right) = \frac{\pi}{2x} \operatorname{erf}(\sqrt{x}) \operatorname{erfi}(\sqrt{x}) - {}_2F_2\left(1, 1; \frac{3}{2}, 2; -x\right), \tag{A18}$$

which one derives from Equation (A5) by partial integration. Hence, for $x \rightarrow \infty$,

$${}_2F_2\left(1, 1; \frac{3}{2}, 2; x\right) \sim \frac{\sqrt{\pi} \exp(x)}{2x^{3/2}} - \frac{\ln(4x) + \gamma}{2x}. \tag{A19}$$

By inserting the asymptotic expansions of Equations (A7), (A13) and (A18) into Equation (A6), one verifies that the singularities for $x_0 \rightarrow \infty$ and $x_1 \rightarrow -\infty$ cancel out as expected, and the final result simplifies to the tractable expression in Equation (17).

References

1. Murray, J.D. *Mathematical Biology*, 2nd ed.; Springer: Berlin/Heidelberg, Germany, 1993.
2. Armitage, J.P. Bacterial tactic responses. *Adv. Microb. Physiol.* **1999**, *41*, 229–289.
3. Adler, J. Chemotaxis in bacteria. *Science* **1966**, *153*, 708–716.
4. Berg, H.C. *E. coli in Motion*; Springer: New York, NY, USA, 2004.
5. Wadhams, G.H.; Armitage, J.P. Making sense of it all: Bacterial chemotaxis. *Nat. Rev. Mol. Cell Biol.* **2004**, *5*, 1024–1037.
6. Schweitzer, F. *Brownian Agents and Active Particles*; Springer: Berlin/Heidelberg, Germany, 2003.
7. Walther, A.; Müller, A.H.E. Janus particles: Synthesis, self-assembly, physical properties, and applications. *Chem. Rev.* **2013**, *113*, 5194–5261.
8. Elgeti, J.; Winkler, R.G.; Gompper, G. Physics of microswimmers—Single particle motion and collective behavior: A review. *Rep. Prog. Phys.* **2015**, *78*, 056601.
9. Bechinger, C.; Di Leonardo, R.; Löwen, H.; Reichhardt, C.; Volpe, G.; Volpe, G. Active particles in complex and crowded environments. *Rev. Mod. Phys.* **2016**, *88*, 045006.
10. Würger, A. Thermophoresis in colloidal suspensions driven by Marangoni forces. *Phys. Rev. Lett.* **2007**, *98*, 138301.
11. Jiang, H.R.; Yoshinaga, N.; Sano, M. Active motion of a Janus particle by self-thermophoresis in a defocused laser beam. *Phys. Rev. Lett.* **2010**, *105*, 268302.
12. Buttinoni, I.; Volpe, G.; Kümmel, F.; Volpe, G.; Bechinger, C. Active Brownian motion tunable by light. *J. Phys. Condens. Matter* **2012**, *24*, 284129.
13. Yang, M.; Ripoll, M. Thermophoretically induced flow field around a colloidal particle. *Soft Matter* **2013**, *9*, 4661–4671.
14. Moran, J.L.; Wheat, P.M.; Posner, J.D. Locomotion of electrocatalytic nanomotors due to reaction induced charge autoelectrophoresis. *Phys. Rev. E* **2010**, *81*, 065302.
15. Ebbens, S.; Gregory, D.A.; Dunderdale, G.; Howse, J.R.; Ibrahim, Y.; Liverpool, T.B.; Golestanian, R. Electrokinetic effects in catalytic platinum-insulator Janus swimmers. *EPL* **2014**, *106*, 58003.
16. Golestanian, R.; Liverpool, T.B.; Ajdari, A. Propulsion of a molecular machine by asymmetric distribution of reaction products. *Phys. Rev. Lett.* **2005**, *94*, 220801.
17. Howse, J.R.; Jones, R.A.L.; Ryan, A.J.; Gough, T.; Vafabakhsh, R.; Golestanian, R. Self-motile colloidal particles: From directed propulsion to random walk. *Phys. Rev. Lett.* **2007**, *99*, 048102.
18. Volpe, G.; Buttinoni, I.; Vogt, D.; Kümmerer, H.J.; Bechinger, C. Microswimmers in patterned environments. *Soft Matter* **2011**, *7*, 8810–8815.
19. Hong, Y.; Blackman, N.M.K.; Kopp, N.D.; Sen, A.; Velegol, D. Chemotaxis of nonbiological colloidal rods. *Phys. Rev. Lett.* **2007**, *99*, 178103.
20. Ghosh, P.K.; Li, Y.; Marchesoni, F.; Nori, F. Pseudochemotactic drifts of artificial microswimmers. *Phys. Rev. E* **2015**, *92*, 012114.
21. Ten Hagen, B.; Kümmel, F.; Wittkowski, R.; Takagi, D.; Löwen, H.; Bechinger, C. Gravitaxis of asymmetric self-propelled colloidal particles. *Nat. Commun.* **2014**, *5*, 4829.
22. Uspal, W.E.; Popescu, M.N.; Dietrich, S.; Tasinkevych, M. Rheotaxis of spherical active particles near a planar wall. *Soft Matter* **2015**, *11*, 6613–6632.
23. Lozano, C.; ten Hagen, B.; Löwen, H.; Bechinger, C. Phototaxis of synthetic microswimmers in optical landscapes. *Nat. Commun.* **2016**, *7*, 12828.
24. Armitage, J.P.; Lackie, J.M. (Eds.) *Biology of the Chemotactic Response*; Cambridge University Press: Cambridge, UK, 1990.
25. Wessels, D.; Murray, J.; Soll, D.R. Behavior of Dictyostelium amoebae is regulated primarily by the temporal dynamic of the natural cAMP wave. *Cell Motil. Cytoskeleton.* **1992**, *23*, 145–156.
26. Stokes, G.G. On the theory of oscillatory waves. *Trans. Camb. Philos. Soc.* **1847**, *8*, 441–473.
27. Van den Broeck, C. Stokes' drift: An exact result. *Europhys. Lett.* **1999**, *46*, 1–5.

28. Höfer, T.; Maini, P.K.; Sherratt, J.A.; Chaplain, M.A.J.; Chauvet, P.; Metevier, D.; Montes, P.C.; Murray, J.D. A resolution of the chemotactic wave paradox. *Appl. Math. Lett.* **1994**, *7*, 1–5.
29. Goldstein, R.E. Traveling-wave chemotaxis. *Phys. Rev. Lett.* **1996**, *77*, 775–778.
30. Geiseler, A.; Hänggi, P.; Marchesoni, F.; Mulhern, C.; Savel'ev, S. Chemotaxis of artificial microswimmers in active density waves. *Phys. Rev. E* **2016**, *94*, 012613.
31. Serdyuk, I.N.; Zaccai, N.R.; Zaccai, J. *Methods in Molecular Biophysics: Structure, Dynamics, Function*; Cambridge University Press: New York, NY, USA, 2007.
32. Ten Hagen, B.; van Teeffelen, S.; Löwen, H. Brownian motion of a self-propelled particle. *J. Phys. Condens. Matter* **2011**, *23*, 194119.
33. Hong, Y.; Velegol, D.; Chaturvedi, N.; Sen, A. Biomimetic behavior of synthetic particles: From microscopic randomness to macroscopic control. *Phys. Chem. Chem. Phys.* **2010**, *12*, 1423–1435.
34. Kapral, R.; Showalter, K. (Eds.) *Chemical Waves and Patterns*; Springer: Dordrecht, The Netherlands, 1995.
35. Thakur, S.; Chen, J.X.; Kapral, R. Interaction of a chemically propelled nanomotor with a chemical wave. *Angew. Chem. Int. Ed.* **2011**, *50*, 10165–10169.
36. Löber, J.; Martens, S.; Engel, H. Shaping wave patterns in reaction-diffusion systems. *Phys. Rev. E* **2014**, *90*, 062911.
37. Navarro, R.M.; Fielding, S.M. Clustering and phase behaviour of attractive active particles with hydrodynamics. *Soft Matter* **2015**, *11*, 7525–7546.
38. Bickel, T.; Zecua, G.; Würger, A. Polarization of active Janus particles. *Phys. Rev. E* **2014**, *89*, 050303.
39. Geiseler, A.; Hänggi, P.; Marchesoni, F. Self-polarizing microswimmers in active density waves. *Sci. Rep.* **2017**, *7*, 41884.
40. Kalinay, P. Effective transport equations in quasi 1D systems. *Eur. Phys. J. Spec. Top.* **2014**, *223*, 3027–3043.
41. Geiseler, A.; Hänggi, P.; Schmid, G. Kramers escape of a self-propelled particle. *Eur. Phys. J. B* **2016**, *89*, 175.
42. Redner, S. *A Guide to First-Passage Processes*; Cambridge University Press: Cambridge, UK, 2001.
43. Goel, N.S.; Richter-Dyn, N. *Stochastic Models in Biology*; Academic Press: New York, NY, USA, 1974.
44. Risken, H. *The Fokker-Planck Equation*, 2nd ed.; Springer: Berlin/Heidelberg, Germany, 1989.
45. Burada, P.S.; Schmid, G.; Reguera, D.; Rubí, J.M.; Hänggi, P. Biased diffusion in confined media: Test of the Fick-Jacobs approximation and validity criteria. *Phys. Rev. E* **2007**, *75*, 051111.
46. Burada, P.S.; Schmid, G.; Hänggi, P. Entropic transport: A test bed for the Fick-Jacobs approximation. *Philos. Trans. R. Soc. A* **2009**, *367*, 3157–3171.
47. Abramowitz, M.; Stegun, I.A. (Eds.) *Handbook of Mathematical Functions*, 10th ed.; U.S. Government Printing Office: Washington, DC, USA, 1972.
48. Mijalkov, M.; McDaniel, A.; Wehr, J.; Volpe, G. Engineering sensorial delay to control phototaxis and emergent collective behaviors. *Phys. Rev. X* **2016**, *6*, 011008.
49. Prudnikov, A.P.; Brychkov, Y.A.; Marichev, O.I. *Integrals and Series. Volume 2: Special Functions*; Gordon and Breach: New York, NY, USA, 1992.
50. Dingle, R.B. Asymptotic expansions and converging factors. II. Error, Dawson, Fresnel, exponential, sine and cosine, and similar integrals. *Proc. R. Soc. A* **1958**, *244*, 476–483.
51. Gradshteyn, I.S.; Ryzhik, I.M. *Table of Integrals, Series, and Products*, 7th ed.; Academic Press: Amsterdam, The Netherlands, 2007.

